BABAR-CONF-03/14
SLAC-PUB-10078
hep-ex/0307087
July 2003

Measurement of Branching Fractions and *CP*-Violating Charge Asymmetries in $B^+ \to \rho^+\pi^0$ and $B^+ \to \rho^0\pi^+$ decays, and Search for $B^0 \to \rho^0\pi^0$

The *BABAR* Collaboration

July 30, 2003

Abstract

We present preliminary measurements of branching fractions and *CP*-violating charge asymmetries in B-meson decays to $\rho\pi$. The data sample comprises 89 million $\Upsilon(4S) \to B\overline{B}$ decays collected with the *BABAR* detector at the PEP-II asymmetric-energy B Factory at SLAC. We find the charge-averaged branching fractions $\mathcal{B}(B^+ \to \rho^+\pi^0) = (11.0 \pm 1.9(\text{stat.}) \pm 1.9(\text{syst.})) \times 10^{-6}$ and $\mathcal{B}(B^+ \to \rho^0\pi^+) = (9.3 \pm 1.0(\text{stat.}) \pm 0.8(\text{syst.})) \times 10^{-6}$; we set a 90% confidence-level upper limit of $\mathcal{B}(B^0 \to \rho^0\pi^0) < 2.5 \times 10^{-6}$. We measure the *CP*-violating charge asymmetries $A_{CP}^{\rho^+\pi^0} = 0.23 \pm 0.16(\text{stat.}) \pm 0.06(\text{syst.})$ and $A_{CP}^{\rho^0\pi^+} = -0.17 \pm 0.11(\text{stat.}) \pm 0.02(\text{syst.})$.

Contributed to the International Europhysics Conference on High Energy Physics
EPS (July 17 - July 23 2003) in Aachen, Germany.

Stanford Linear Accelerator Center, Stanford University, Stanford, CA 94309

Work supported in part by U.S. Department of Energy contract DE-AC03-76SF00515.

The *BABAR* Collaboration,

B. Aubert, R. Barate, D. Boutigny, J.-M. Gaillard, A. Hicheur, Y. Karyotakis, J. P. Lees, P. Robbe, V. Tisserand, A. Zghiche

Laboratoire de Physique des Particules, F-74941 Annecy-le-Vieux, France

A. Palano, A. Pompili

Università di Bari, Dipartimento di Fisica and INFN, I-70126 Bari, Italy

J. C. Chen, N. D. Qi, G. Rong, P. Wang, Y. S. Zhu

Institute of High Energy Physics, Beijing 100039, China

G. Eigen, I. Ofte, B. Stugu

University of Bergen, Inst. of Physics, N-5007 Bergen, Norway

G. S. Abrams, A. W. Borgland, A. B. Breon, D. N. Brown, J. Button-Shafer, R. N. Cahn, E. Charles, C. T. Day, M. S. Gill, A. V. Gritsan, Y. Groysman, R. G. Jacobsen, R. W. Kadel, J. Kadyk, L. T. Kerth, Yu. G. Kolomensky, J. F. Kral, G. Kukartsev, C. LeClerc, M. E. Levi, G. Lynch, L. M. Mir, P. J. Oddone, T. J. Orimoto, M. Pripstein, N. A. Roe, A. Romosan, M. T. Ronan, V. G. Shelkov, A. V. Telnov, W. A. Wenzel

Lawrence Berkeley National Laboratory and University of California, Berkeley, CA 94720, USA

K. Ford, T. J. Harrison, C. M. Hawkes, D. J. Knowles, S. E. Morgan, R. C. Penny, A. T. Watson, N. K. Watson

University of Birmingham, Birmingham, B15 2TT, United Kingdom

T. Deppermann, K. Goetzen, H. Koch, B. Lewandowski, M. Pelizaeus, K. Peters, H. Schmuecker, M. Steinke

Ruhr Universität Bochum, Institut für Experimentalphysik 1, D-44780 Bochum, Germany

N. R. Barlow, J. T. Boyd, N. Chevalier, W. N. Cottingham, M. P. Kelly, T. E. Latham, C. Mackay, F. F. Wilson

University of Bristol, Bristol BS8 1TL, United Kingdom

K. Abe, T. Cuhadar-Donszelmann, C. Hearty, T. S. Mattison, J. A. McKenna, D. Thiessen

University of British Columbia, Vancouver, BC, Canada V6T 1Z1

P. Kyberd, A. K. McKemey

Brunel University, Uxbridge, Middlesex UB8 3PH, United Kingdom

V. E. Blinov, A. D. Bukin, V. B. Golubev, V. N. Ivanchenko, E. A. Kravchenko, A. P. Onuchin, S. I. Serednyakov, Yu. I. Skovpen, E. P. Solodov, A. N. Yushkov

Budker Institute of Nuclear Physics, Novosibirsk 630090, Russia

D. Best, M. Bruinsma, M. Chao, D. Kirkby, A. J. Lankford, M. Mandelkern, R. K. Mommsen, W. Roethel, D. P. Stoker

University of California at Irvine, Irvine, CA 92697, USA

C. Buchanan, B. L. Hartfiel

University of California at Los Angeles, Los Angeles, CA 90024, USA

B. C. Shen

University of California at Riverside, Riverside, CA 92521, USA

D. del Re, H. K. Hadavand, E. J. Hill, D. B. MacFarlane, H. P. Paar, Sh. Rahatlou, U. Schwanke, V. Sharma

University of California at San Diego, La Jolla, CA 92093, USA

J. W. Berryhill, C. Campagnari, B. Dahmes, N. Kuznetsova, S. L. Levy, O. Long, A. Lu, M. A. Mazur, J. D. Richman, W. Verkerke

University of California at Santa Barbara, Santa Barbara, CA 93106, USA

T. W. Beck, J. Beringer, A. M. Eisner, C. A. Heusch, W. S. Lockman, T. Schalk, R. E. Schmitz, B. A. Schumm, A. Seiden, M. Turri, W. Walkowiak, D. C. Williams, M. G. Wilson

University of California at Santa Cruz, Institute for Particle Physics, Santa Cruz, CA 95064, USA

J. Albert, E. Chen, G. P. Dubois-Felsmann, A. Dvoretskii, D. G. Hitlin, I. Narsky, F. C. Porter, A. Ryd, A. Samuel, S. Yang

California Institute of Technology, Pasadena, CA 91125, USA

S. Jayatilleke, G. Mancinelli, B. T. Meadows, M. D. Sokoloff

University of Cincinnati, Cincinnati, OH 45221, USA

T. Abe, F. Blanc, P. Bloom, S. Chen, P. J. Clark, W. T. Ford, U. Nauenberg, A. Olivas, P. Rankin, J. Roy, J. G. Smith, W. C. van Hoek, L. Zhang

University of Colorado, Boulder, CO 80309, USA

J. L. Harton, T. Hu, A. Soffer, W. H. Toki, R. J. Wilson, J. Zhang

Colorado State University, Fort Collins, CO 80523, USA

D. Altenburg, T. Brandt, J. Brose, T. Colberg, M. Dickopp, R. S. Dubitzky, A. Hauke, H. M. Lacker, E. Maly, R. Müller-Pfefferkorn, R. Nogowski, S. Otto, J. Schubert, K. R. Schubert, R. Schwierz, B. Spaan, L. Wilden

Technische Universität Dresden, Institut für Kern- und Teilchenphysik, D-01062 Dresden, Germany

D. Bernard, G. R. Bonneaud, F. Brochard, J. Cohen-Tanugi, P. Grenier, Ch. Thiebaux, G. Vasileiadis, M. Verderi

Ecole Polytechnique, LLR, F-91128 Palaiseau, France

A. Khan, D. Lavin, F. Muheim, S. Playfer, J. E. Swain, J. Tinslay

University of Edinburgh, Edinburgh EH9 3JZ, United Kingdom

M. Andreotti, V. Azzolini, D. Bettoni, C. Bozzi, R. Calabrese, G. Cibinetto, E. Luppi, M. Negrini, L. Piemontese, A. Sarti

Università di Ferrara, Dipartimento di Fisica and INFN, I-44100 Ferrara, Italy

E. Treadwell

Florida A&M University, Tallahassee, FL 32307, USA

F. Anulli,[1] R. Baldini-Ferroli, M. Biasini,[1] A. Calcaterra, R. de Sangro, D. Falciai, G. Finocchiaro, P. Patteri, I. M. Peruzzi,[1] M. Piccolo, M. Pioppi,[1] A. Zallo

Laboratori Nazionali di Frascati dell'INFN, I-00044 Frascati, Italy

A. Buzzo, R. Capra, R. Contri, G. Crosetti, M. Lo Vetere, M. Macri, M. R. Monge, S. Passaggio, C. Patrignani, E. Robutti, A. Santroni, S. Tosi

Università di Genova, Dipartimento di Fisica and INFN, I-16146 Genova, Italy

S. Bailey, M. Morii, E. Won

Harvard University, Cambridge, MA 02138, USA

W. Bhimji, D. A. Bowerman, P. D. Dauncey, U. Egede, I. Eschrich, J. R. Gaillard, G. W. Morton, J. A. Nash, P. Sanders, G. P. Taylor

Imperial College London, London, SW7 2BW, United Kingdom

G. J. Grenier, S.-J. Lee, U. Mallik

University of Iowa, Iowa City, IA 52242, USA

J. Cochran, H. B. Crawley, J. Lamsa, W. T. Meyer, S. Prell, E. I. Rosenberg, J. Yi

Iowa State University, Ames, IA 50011-3160, USA

M. Davier, G. Grosdidier, A. Höcker, S. Laplace, F. Le Diberder, V. Lepeltier, A. M. Lutz, T. C. Petersen, S. Plaszczynski, M. H. Schune, L. Tantot, G. Wormser

Laboratoire de l'Accélérateur Linéaire, F-91898 Orsay, France

V. Brigljević , C. H. Cheng, D. J. Lange, D. M. Wright

Lawrence Livermore National Laboratory, Livermore, CA 94550, USA

A. J. Bevan, J. P. Coleman, J. R. Fry, E. Gabathuler, R. Gamet, M. Kay, R. J. Parry, D. J. Payne, R. J. Sloane, C. Touramanis

University of Liverpool, Liverpool L69 3BX, United Kingdom

J. J. Back, P. F. Harrison, H. W. Shorthouse, P. Strother, P. B. Vidal

Queen Mary, University of London, E1 4NS, United Kingdom

C. L. Brown, G. Cowan, R. L. Flack, H. U. Flaecher, S. George, M. G. Green, A. Kurup, C. E. Marker, T. R. McMahon, S. Ricciardi, F. Salvatore, G. Vaitsas, M. A. Winter

University of London, Royal Holloway and Bedford New College, Egham, Surrey TW20 0EX, United Kingdom

D. Brown, C. L. Davis

University of Louisville, Louisville, KY 40292, USA

J. Allison, R. J. Barlow, A. C. Forti, P. A. Hart, F. Jackson, G. D. Lafferty, A. J. Lyon, J. H. Weatherall, J. C. Williams

University of Manchester, Manchester M13 9PL, United Kingdom

A. Farbin, A. Jawahery, D. Kovalskyi, C. K. Lae, V. Lillard, D. A. Roberts

University of Maryland, College Park, MD 20742, USA

[1]Also with Università di Perugia, Perugia, Italy

G. Blaylock, C. Dallapiccola, K. T. Flood, S. S. Hertzbach, R. Kofler, V. B. Koptchev, T. B. Moore, S. Saremi, H. Staengle, S. Willocq

University of Massachusetts, Amherst, MA 01003, USA

R. Cowan, G. Sciolla, F. Taylor, R. K. Yamamoto

Massachusetts Institute of Technology, Laboratory for Nuclear Science, Cambridge, MA 02139, USA

D. J. J. Mangeol, M. Milek, P. M. Patel

McGill University, Montréal, QC, Canada H3A 2T8

A. Lazzaro, F. Palombo

Università di Milano, Dipartimento di Fisica and INFN, I-20133 Milano, Italy

J. M. Bauer, L. Cremaldi, V. Eschenburg, R. Godang, R. Kroeger, J. Reidy, D. A. Sanders, D. J. Summers, H. W. Zhao

University of Mississippi, University, MS 38677, USA

S. Brunet, D. Cote-Ahern, C. Hast, P. Taras

Université de Montréal, Laboratoire René J. A. Lévesque, Montréal, QC, Canada H3C 3J7

H. Nicholson

Mount Holyoke College, South Hadley, MA 01075, USA

C. Cartaro, N. Cavallo,[2] G. De Nardo, F. Fabozzi,[2] C. Gatto, L. Lista, P. Paolucci, D. Piccolo, C. Sciacca

Università di Napoli Federico II, Dipartimento di Scienze Fisiche and INFN, I-80126, Napoli, Italy

M. A. Baak, G. Raven

NIKHEF, National Institute for Nuclear Physics and High Energy Physics, NL-1009 DB Amsterdam, The Netherlands

J. M. LoSecco

University of Notre Dame, Notre Dame, IN 46556, USA

T. A. Gabriel

Oak Ridge National Laboratory, Oak Ridge, TN 37831, USA

B. Brau, K. K. Gan, K. Honscheid, D. Hufnagel, H. Kagan, R. Kass, T. Pulliam, Q. K. Wong

Ohio State University, Columbus, OH 43210, USA

J. Brau, R. Frey, C. T. Potter, N. B. Sinev, D. Strom, E. Torrence

University of Oregon, Eugene, OR 97403, USA

F. Colecchia, A. Dorigo, F. Galeazzi, M. Margoni, M. Morandin, M. Posocco, M. Rotondo, F. Simonetto, R. Stroili, G. Tiozzo, C. Voci

Università di Padova, Dipartimento di Fisica and INFN, I-35131 Padova, Italy

M. Benayoun, H. Briand, J. Chauveau, P. David, Ch. de la Vaissière, L. Del Buono, O. Hamon, M. J. J. John, Ph. Leruste, J. Ocariz, M. Pivk, L. Roos, J. Stark, S. T'Jampens, G. Therin

Universités Paris VI et VII, Lab de Physique Nucléaire H. E., F-75252 Paris, France

[2]Also with Università della Basilicata, Potenza, Italy

P. F. Manfredi, V. Re

Università di Pavia, Dipartimento di Elettronica and INFN, I-27100 Pavia, Italy

P. K. Behera, L. Gladney, Q. H. Guo, J. Panetta

University of Pennsylvania, Philadelphia, PA 19104, USA

C. Angelini, G. Batignani, S. Bettarini, M. Bondioli, F. Bucci, G. Calderini, M. Carpinelli, F. Forti, M. A. Giorgi, A. Lusiani, G. Marchiori, F. Martinez-Vidal,[3] M. Morganti, N. Neri, E. Paoloni, M. Rama, G. Rizzo, F. Sandrelli, J. Walsh

Università di Pisa, Dipartimento di Fisica, Scuola Normale Superiore and INFN, I-56127 Pisa, Italy

M. Haire, D. Judd, K. Paick, D. E. Wagoner

Prairie View A&M University, Prairie View, TX 77446, USA

N. Danielson, P. Elmer, C. Lu, V. Miftakov, J. Olsen, A. J. S. Smith, H. A. Tanaka, E. W. Varnes

Princeton University, Princeton, NJ 08544, USA

F. Bellini, G. Cavoto,[4] R. Faccini,[5] F. Ferrarotto, F. Ferroni, M. Gaspero, M. A. Mazzoni, S. Morganti, M. Pierini, G. Piredda, F. Safai Tehrani, C. Voena

Università di Roma La Sapienza, Dipartimento di Fisica and INFN, I-00185 Roma, Italy

S. Christ, G. Wagner, R. Waldi

Universität Rostock, D-18051 Rostock, Germany

T. Adye, N. De Groot, B. Franek, N. I. Geddes, G. P. Gopal, E. O. Olaiya, S. M. Xella

Rutherford Appleton Laboratory, Chilton, Didcot, Oxon, OX11 0QX, United Kingdom

R. Aleksan, S. Emery, A. Gaidot, S. F. Ganzhur, P.-F. Giraud, G. Hamel de Monchenault, W. Kozanecki, M. Langer, M. Legendre, G. W. London, B. Mayer, G. Schott, G. Vasseur, Ch. Yeche, M. Zito

DSM/Dapnia, CEA/Saclay, F-91191 Gif-sur-Yvette, France

M. V. Purohit, A. W. Weidemann, F. X. Yumiceva

University of South Carolina, Columbia, SC 29208, USA

D. Aston, R. Bartoldus, N. Berger, A. M. Boyarski, O. L. Buchmueller, M. R. Convery, D. P. Coupal, D. Dong, J. Dorfan, D. Dujmic, W. Dunwoodie, R. C. Field, T. Glanzman, S. J. Gowdy, E. Grauges-Pous, T. Hadig, V. Halyo, T. Hryn'ova, W. R. Innes, C. P. Jessop, M. H. Kelsey, P. Kim, M. L. Kocian, U. Langenegger, D. W. G. S. Leith, S. Luitz, V. Luth, H. L. Lynch, H. Marsiske, R. Messner, D. R. Muller, C. P. O'Grady, V. E. Ozcan, A. Perazzo, M. Perl, S. Petrak, B. N. Ratcliff, S. H. Robertson, A. Roodman, A. A. Salnikov, R. H. Schindler, J. Schwiening, G. Simi, A. Snyder, A. Soha, J. Stelzer, D. Su, M. K. Sullivan, J. Va'vra, S. R. Wagner, M. Weaver, A. J. R. Weinstein, W. J. Wisniewski, D. H. Wright, C. C. Young

Stanford Linear Accelerator Center, Stanford, CA 94309, USA

P. R. Burchat, A. J. Edwards, T. I. Meyer, B. A. Petersen, C. Roat

Stanford University, Stanford, CA 94305-4060, USA

[3] Also with IFIC, Instituto de Física Corpuscular, CSIC-Universidad de Valencia, Valencia, Spain

[4] Also with Princeton University

[5] Also with University of California at San Diego

S. Ahmed, M. S. Alam, J. A. Ernst, M. Saleem, F. R. Wappler
State Univ. of New York, Albany, NY 12222, USA

W. Bugg, M. Krishnamurthy, S. M. Spanier
University of Tennessee, Knoxville, TN 37996, USA

R. Eckmann, H. Kim, J. L. Ritchie, R. F. Schwitters
University of Texas at Austin, Austin, TX 78712, USA

J. M. Izen, I. Kitayama, X. C. Lou, S. Ye
University of Texas at Dallas, Richardson, TX 75083, USA

F. Bianchi, M. Bona, F. Gallo, D. Gamba
Università di Torino, Dipartimento di Fisica Sperimentale and INFN, I-10125 Torino, Italy

C. Borean, L. Bosisio, G. Della Ricca, S. Dittongo, S. Grancagnolo, L. Lanceri, P. Poropat,[6] L. Vitale, G. Vuagnin
Università di Trieste, Dipartimento di Fisica and INFN, I-34127 Trieste, Italy

R. S. Panvini
Vanderbilt University, Nashville, TN 37235, USA

Sw. Banerjee, C. M. Brown, D. Fortin, P. D. Jackson, R. Kowalewski, J. M. Roney
University of Victoria, Victoria, BC, Canada V8W 3P6

H. R. Band, S. Dasu, M. Datta, A. M. Eichenbaum, J. R. Johnson, P. E. Kutter, H. Li, R. Liu, F. Di Lodovico, A. Mihalyi, A. K. Mohapatra, Y. Pan, R. Prepost, S. J. Sekula, J. H. von Wimmersperg-Toeller, J. Wu, S. L. Wu, Z. Yu
University of Wisconsin, Madison, WI 53706, USA

H. Neal
Yale University, New Haven, CT 06511, USA

[6] Deceased

1 Introduction

The study of B meson decays into charmless hadronic final states plays an important role in the understanding of the phenomenon of *CP* violation in the B system. Recently, the *BABAR* experiment has performed a search for *CP*-violating asymmetries in neutral B decays to $\rho^{\pm}\pi^{\mp}$ [1], where the mixing-induced *CP* asymmetry is related to the angle $\alpha \equiv \arg\left[-V_{td}V_{tb}^{*}/V_{ud}V_{ub}^{*}\right]$ of the Unitarity Triangle. However, in contrast to the theoretically clean determination of $\sin 2\beta$ in the decay to charmonium such as $B^0 \to J/\psi K_S^0$ [2, 3], the extraction of α from $\rho^{\pm}\pi^{\mp}$ is complicated by the interference of decay amplitudes with different weak phases. Various strategies to overcome this problem have been proposed in the literature. One such method is an SU(2) isospin analysis of the $\rho\pi$ final states [4]. In the limit of isospin symmetry, the five decay amplitudes $B^0 \to \rho^+\pi^-$, $B^0 \to \rho^-\pi^+$, $B^0 \to \rho^0\pi^0$, $B^+ \to \rho^+\pi^0$ and $B^+ \to \rho^0\pi^+$ form a pentagon in the complex plane. Combining measurements of all the decay rates, mixing-induced and direct *CP* asymmetries in the neutral B modes, as well as charge asymmetries in the charged B modes, allows a determination of the phase α that is free of hadronic uncertainties.

In this letter, we present preliminary measurements of the branching fractions of the decay modes[7] $B^+ \to \rho^0\pi^+$, $B^+ \to \rho^+\pi^0$, and perform a search for the decay $B^0 \to \rho^0\pi^0$. For the charged modes we also present measurements of the *CP*-violating charge asymmetry A_{CP}, defined by

$$A_{CP} \equiv \frac{\Gamma(B^- \to f) - \Gamma(B^+ \to \bar{f})}{\Gamma(B^- \to f) + \Gamma(B^+ \to \bar{f})} \tag{1}$$

where $\Gamma(B^- \to f)$ and $\Gamma(B^+ \to \bar{f})$ are the B^- and B^+ decay rates, respectively. A non-zero A_{CP} requires the presence of at least two amplitudes with different weak and strong phases.

The measurements of the branching fractions and charge asymmetries use events collected by the *BABAR* detector at the PEP-II asymmetric-energy B Factory. The sample used for the charged modes consists of 88.5×10^6 $B\overline{B}$ pairs collected at the $\Upsilon(4S)$ resonance ("on-resonance"), while the $B^0 \to \rho^0\pi^0$ search uses a slightly larger sample of 88.9×10^6 $B\overline{B}$ pairs. We use an integrated luminosity of $9.6\,\mathrm{fb}^{-1}$ collected approximately 40 MeV below the $\Upsilon(4S)$ ("off-resonance") for background studies. We determine the yields and charge asymmetries using a maximum likelihood (ML) fit.

2 The *BABAR* Detector

A detailed description of the *BABAR* detector can be found in Ref. [5]. Charged-particle momenta are measured in a tracking system consisting of a 5-layer double-sided silicon vertex tracker (SVT) and a 40-layer drift chamber (DCH) filled with a gas mixture based on helium and isobutane. The SVT and DCH operate within a 1.5 T superconducting solenoidal magnet. The typical decay vertex resolution is around $65\,\mu$m along the beam direction for the fully-reconstructed $B_{\rho\pi}$ (referred to as signal B hereafter), and around $185\,\mu$m for the inclusively-reconstructed rest of the event. Photons are detected in an electromagnetic calorimeter (EMC) consisting of 6580 CsI(Tl) crystals arranged in barrel and forward end-cap sub-detectors. The average π^0 mass resolution is $7\,\mathrm{MeV}/c^2$. The flux return for the solenoid is composed of multiple layers of iron and resistive plate chambers for the identification of muons and long-lived neutral hadrons. Tracks are identified as pions, kaons or protons by the Cherenkov angle θ_C measured with a detector of internally reflected Cherenkov

[7] If not stated otherwise, charge conjugation is implied throughout this document.

light (DIRC). The typical separation between pions and kaons varies from 8σ at $2\,\mathrm{GeV}/c$ to 2.5σ at $4\,\mathrm{GeV}/c$, where σ is the average θ_C resolution. Lower momentum kaons are identified with a combination of θ_C (for momenta down to $0.7\,\mathrm{GeV}/c$) and measurements of energy loss, dE/dx, in the DCH and SVT.

3 Discriminating Variables

To reject background from continuum $e^+e^- \to q\bar{q}$ ($q = u, d, s, c$) events and other B decays, we use the following discriminating variables:

- m_{ES}: the beam-energy-substituted mass is defined by

$$m_{ES} = \sqrt{(s/2 + \mathbf{p}_i \cdot \mathbf{p}_B)^2/E_i^2 - \mathbf{p}_B^2}\ , \tag{2}$$

  where s is the square of the center-of-mass (CM) energy, E_i and $\mathbf{p}_i$ are the total energy and three-momentum of the initial e^+e^- state in the laboratory frame, and $\mathbf{p}_B$ is the three-momentum of the B candidate in the same frame. Signal events populate the m_{ES} region near the B mass. Background events usually have a wider or even flat m_{ES} distribution.

- ΔE: the difference between the reconstructed energy of the signal B candidate and the beam energy in the CM frame. The ΔE distribution for signal events peaks around zero. Backgrounds from other B-meson decays peak at different ΔE depending on the number of charged and neutral particles in the decay. Two-body and four-body decays populate the positive and negative regions of ΔE, respectively, while three-body decays have ΔE values near zero. The ΔE is shifted if a misidentified charged track is used to reconstruct the signal B.

- Output of a multivariate analyzer : the dominant background for charmless B decays are continuum events. To enhance discrimination between signal and continuum, three neural networks (NN), one for each signal mode, are constructed. Each NN is trained with off-resonance data and simulated events of its corresponding signal. All NNs use: the reconstructed ρ mass; $\cos\theta_\pi$, where θ_π is the angle between the momentum of the $\pi^+(\pi^0)$ from the $\rho^0(\rho^+)$ decay and the B momentum in the ρ rest frame; the event shape variables $L_0 = \sum_i p_i^*$ and $L_2 = \sum_i p_i^* \times |\cos(\theta^*_{T_B,i})|^2$, where p_i^* is the CM momentum of the track or neutral object i, belonging to the rest of the event, and $\theta^*_{T_B,i}$ is the angle between the momentum of track i and the B thrust axis T_B in the CM frame; $|\cos(\theta_{B,z})|$, the cosine of the angle between the B momentum and the z axis (along the beam direction) in the CM frame, and $|\cos(\theta_{T_B,z})|$, the cosine of the angle between the B thrust axis and the z axis in the CM frame.

4 Event Selection and Reconstruction

Signal B candidates are reconstructed from combinations of three-pion final states that must be $\pi^+\pi^0\pi^0$ for $B^+ \to \rho^+\pi^0$, $\pi^+\pi^-\pi^+$ for $B^+ \to \rho^0\pi^+$, and $\pi^+\pi^-\pi^0$ for $B^0 \to \rho^0\pi^0$. The charged tracks must be inconsistent with being an electron based on dE/dx measurements, shower shape criteria in the EMC, and the ratio of shower energy and track momentum. Charged tracks must also be inconsistent with being a kaon or a proton. The photon candidates used to form a π^0 must have an energy greater than $50\,\mathrm{MeV}$ in the laboratory frame, and exhibit a lateral shower profile

of energy deposition in the EMC consistent with an electromagnetic shower. The invariant mass $m(\gamma\gamma)$ of the photon pair must satisfy $0.11 < m(\gamma\gamma) < 0.16\,\mathrm{GeV}/c^2$.

Two of the three final state pions are used to form a charged or a neutral ρ candidate (the third pion is referred to as the bachelor pion hereafter). For the $B^+ \to \rho^+\pi^0$ mode, the ρ^+ candidate is reconstructed from the positively charged track and one of the two π^0 candidates. For the $B^+ \to \rho^0\pi^+$ and $B^0 \to \rho^0\pi^0$ modes, the ρ^0 candidate is reconstructed from two oppositely-charged tracks. The mass of the ρ candidates must satisfy $0.4 < m(\pi^+\pi^0) < 1.3\,\mathrm{GeV}/c^2$ for $B^+ \to \rho^+\pi^0$, $0.53 < m(\pi^+\pi^-) < 0.9\,\mathrm{GeV}/c^2$ for $B^+ \to \rho^0\pi^+$, and $0.4 < m(\pi^+\pi^-) < 0.9\,\mathrm{GeV}/c^2$ for $B^0 \to \rho^0\pi^0$. The $B^+ \to \rho^0\pi^+$ mass cut has been tightened to remove B-related backgrounds such as $B^+ \to f_0(980)\pi^+(K^+)$, $K^0_S\pi^+$. The $B^0 \to \rho^0\pi^0$ mass cut is tight to remove $B^0 \to f_0(980)\pi^0$. For the $B^0 \to \rho^0\pi^0$ mode, the corners of the Dalitz plot where $\rho^0\pi^0$ interferes with the dominant $\rho^\pm\pi^\mp$ are removed by requiring that the invariant masses $m(\pi^+\pi^0)$ and $m(\pi^-\pi^0)$ be greater than $1.3\,\mathrm{GeV}/c^2$. To take advantage of the helicity structure of $B \to \rho\pi$ decays, we require $|\cos\theta_\pi| > 0.25$.

To reject background from $B^+ \to \rho^0 K^+$ and $B^0 \to \rho^- K^+$ decays, only $\rho^0\pi^+$ candidates with bachelor tracks within the geometrical acceptance of the DIRC are considered. The number of photons in the DIRC that are associated with the bachelor track must not be less than 5.

For the $B^+ \to \rho^+\pi^0$ and $B^0 \to \rho^0\pi^0$ modes, the invariant mass of either track and the π^0 must be less than $5.14\,\mathrm{GeV}/c^2$ to reject two-body B background.

B candidates are required to satisfy kinematic fit-region cuts. For $B^+ \to \rho^+\pi^0$ decays, candidates must satisfy $5.20 < m_{ES} < 5.29\,\mathrm{GeV}/c^2$ and $-0.15 < \Delta E < 0.10\,\mathrm{GeV}$. $B^+ \to \rho^0\pi^+$ candidates must satisfy $5.23 < m_{ES} < 5.29\,\mathrm{GeV}/c^2$ and $-0.05 < \Delta E < 0.05\,\mathrm{GeV}$. The $B^+ \to \rho^0\pi^+$ analysis benefits from a better ΔE resolution due to the absence of neutral pions; the tight cut on ΔE helps to remove four-body B background more effectively. $B^0 \to \rho^0\pi^0$ candidates must satisfy $5.23 < m_{ES} < 5.29\,\mathrm{GeV}/c^2$ and $-0.15 < \Delta E < 0.10\,\mathrm{GeV}$.

For the $B^+ \to \rho^0\pi^+$ mode, we remove background from charmed decays $B \to \overline{D}^0 X$, $\overline{D}^0 \to K^+\pi^-$ or $\pi^+\pi^-$, by requiring that all pairs of oppositely-charged tracks have invariant masses either smaller than $1.844\,\mathrm{GeV}/c^2$ or greater than $1.884\,\mathrm{GeV}/c^2$, assuming both kaon and pion hypotheses for the positively-charged track.

The final samples of signal candidates are selected with a cut on the NN outputs for all three decay modes. For example, the NN cut for the $B^+ \to \rho^0\pi^+$ decay mode retains 85%(11%) of the signal (continuum) events.

In each event, final state particles other than the three pions that form the signal B meson are assumed to belong to the other B meson. These particles are used to tag the flavor of the other B meson and to inclusively-reconstruct its vertex for decay time determination. In this letter, this other B is referred to as B_{tag}.

For the $B^0 \to \rho^0\pi^0$ mode, we use the proper decay time as a discriminating variable in the ML fit. The time difference Δt is obtained from the measured distance between the z positions (along the beam direction) of the $B_{\rho^0\pi^0}$ and B_{tag} decay vertices, and the known boost of the e^+e^- system. The vertex of the B_{tag} is reconstructed from all tracks in the event except those from the $B_{\rho^0\pi^0}$, and an iterative procedure [2] is used to remove tracks with a large contribution to the vertex χ^2. An additional constraint is obtained from the three-momentum and vertex position of the $B_{\rho^0\pi^0}$ candidate, and the average e^+e^- interaction point and boost. We require $|\Delta t| < 20\,\mathrm{ps}$ and $\sigma(\Delta t) < 2.5\,\mathrm{ps}$, where $\sigma(\Delta t)$ is the error on Δt estimated on an event-by-event basis.

Approximately 33% (7% and 8%) of the events from signal Monte Carlo (MC) simulation have more than one candidate satisfying the selection in the $B^+ \to \rho^+\pi^0$ ($B^+ \to \rho^0\pi^+$ and $B^0 \to \rho^0\pi^0$) decay mode. In this case, we choose the candidate with the reconstructed ρ invariant mass closest

Table 1: *Signal efficiencies (ϵ), fractions of misreconstructed signal events ($f_{\rm scf}$), and fractions of misreconstructed signal events with wrong B candidate charge (ω_Q) in selected MC-simulated events. The last row gives the numbers of selected on-resonance events entering the maximum likelihood fits.*

	$B^+ \to \rho^+\pi^0$	$B^+ \to \rho^0\pi^+$	$B^0 \to \rho^0\pi^0$
ϵ [%]	17.6 ± 0.1	29.0 ± 0.1	20.2 ± 0.1
$f_{\rm scf}$ [%]	38.6 ± 0.2	7.1 ± 0.1	9.4 ± 0.2
ω_Q [%]	8.1 ± 0.1	1.6 ± 0.1	-
Selected events	13104	8498	6648

to the nominal ρ mass [6]. Any chosen candidate from a signal event that is reconstructed from one or more wrong particles (charged or neutral) is hereafter referred to as misreconstructed signal.

The signal selection efficiencies are determined by applying the selection criteria to MC. Efficiencies (including misreconstructed signal) of the three decay modes are summarized in Table 1. Also given in Table 1 are the fractions of misreconstructed events in the selected signal samples. Misreconstruction is mostly due to ρ candidates that include a random low-momentum pion. Some of the misreconstructed events are assigned an incorrect B charge in charged B decays. The total number of events that enter the likelihood fits are given in the last row of Table 1.

While flavor information of the $B_{\rm tag}$ is not explicitly used in our analyses, event properties used to categorize flavor-tagged events can be exploited to distinguish signal and (mainly) continuum background because they populate among tagging categories in dramatically different ways. Five mutually exclusive tagging categories are defined: `Lepton`, `Kaon`, `NT1`, `NT2`, and `Untagged`. They are determined by a tagging algorithm [2] relying on the correlation between the flavor of the b quark and the charge of the remaining tracks in the event, after removal of the tracks from the $B \to \rho\pi$. The fractions of signal events in each tagging category are measured from data using a control sample of fully-reconstructed B decays [2]. Tagging fractions for B backgrounds are taken from Monte Carlo. Separate continuum background yields for each category are free to vary in the maximum likelihood fit. Using tagging categories, we decrease the statistical error in the signal yield by about 10%.

5 *B*-related Backgrounds

We use MC simulation to study the cross-feed from two-body, three-body and four-body charmless B decays, as well as from inclusive $b \to c$ decays. The branching fractions of unmeasured decay channels are estimated within conservative error ranges. The charmless modes are grouped into eighteen ($B^+ \to \rho^+\pi^0$), fifteen ($B^+ \to \rho^0\pi^+$) and seventeen ($B^0 \to \rho^0\pi^0$) classes with similar kinematic and topological properties. Two additional classes account for the neutral and charged $b \to c$ decays. For each of the background classes, a component is introduced into the ML fit, with a fixed number of events. Contributions to the systematic error by each B background mode is obtained by varying its yield by one standard deviation. For unknown modes with only estimated branching ratios, the uncertainties are divided by $\sqrt{3}$ and taken as the standard deviations. Tables 2, 3 and

4 summarize the dominant B background modes to $B^+ \to \rho^+\pi^0$, $B^+ \to \rho^0\pi^+$ and $B^0 \to \rho^0\pi^0$, respectively.

6 The Likelihood

We use unbinned extended maximum likelihood fits to extract the $\rho\pi$ event yields, the charge asymmetries, and other parameters used to model signal and background events. The fits minimize the quantity $-2\ln\mathcal{L}$, where $\mathcal{L}$ is the total likelihood defined over all tagging categories k by

$$\mathcal{L} = \prod_k e^{-N'_k} \prod_{i=1}^{N_k} \mathcal{L}_{i,\,k} \ , \tag{3}$$

and where N'_k is the sum of the signal and continuum yields (to be determined by the fit) and the fixed B-background yields, N_k are the numbers of observed events in category k, and $\mathcal{L}_{i,\,k}$ is the likelihood computed for event i. Note that no tagging information is used in the $B^+ \to \rho^0\pi^+$ fit. The data sample of each mode is assumed to consist of signal, continuum background and B-background components. The variables m_{ES}, ΔE and the NN output discriminate signal from background. For $B^0 \to \rho^0\pi^0$, the variable Δt is used to obtain additional background discrimination.

The likelihood $\mathcal{L}_{i,\,k}$ for event i is the sum of the probability density functions (PDF) of all components, weighted by the expected yields for each component,

$$\mathcal{L}_{i,\,k} = N^{\rho\pi}\epsilon_k\mathcal{P}^{\rho\pi}_{i,\,k} + N^{q\bar{q}}_k\mathcal{P}^{q\bar{q}}_{i,\,k} + \sum_{j=1}^{N_B}\mathcal{L}^B_{ij,\,k} \ , \tag{4}$$

where

- $N^{\rho\pi}$ is the number of signal events in the entire sample. For the $\rho^+\pi^0$ and $\rho^0\pi^+$ modes, the charge asymmetries are introduced by multiplying the signal yields by $\frac{1}{2}(1 - Q_B A_{CP})$, where Q_B is the charge of B candidate.
- ϵ_k is the fraction of signal events that are tagged in category k.
- $N^{q\bar{q}}_k$ is the expected number of continuum background events that are tagged in category k.
- The PDFs $\mathcal{P}^{\rho\pi}_k$, $\mathcal{P}^{q\bar{q}}_k$ and the likelihood terms $\mathcal{L}^B_{j,k}$ are the product of the PDFs of the discriminating variables. The signal PDFs are thus given by $\mathcal{P}^{(\rho\pi)^+}_k \equiv \mathcal{P}^{(\rho\pi)+}(m_{ES}) \cdot \mathcal{P}^{(\rho\pi)+}(\Delta E) \cdot \mathcal{P}^{(\rho\pi)+}_k(\mathrm{NN})$ for the charged B decay modes, and by $\mathcal{P}^{\rho^0\pi^0}_k \equiv \mathcal{P}^{\rho^0\pi^0}(m_{ES}) \cdot \mathcal{P}^{\rho^0\pi^0}(\Delta E) \cdot \mathcal{P}^{\rho^0\pi^0}_k(\mathrm{NN}) \cdot \mathcal{P}^{\rho^0\pi^0}_k(\Delta t)$ for $B^0 \to \rho^0\pi^0$. The PDF for continuum events is denoted $\mathcal{P}^{q\bar{q}}_{i,\,k}$. The likelihood term $\mathcal{L}^B_{ij,\,k}$ corresponds to the j_{th} $B\overline{B}$ background's contribution of the N_B B background categories. Correlations between the variables are usually neglected except that for B backgrounds we use two-dimensional PDFs for m_{ES} and ΔE to model the sizable correlations.

The signal PDFs are decomposed into two parts with distinct distributions: signal events that are correctly reconstructed and misreconstructed signal events. Moreover, for the charged B modes we distinguish misreconstructed signal events with right-sign B charge from those with wrong-sign B charge in the likelihood. Their individual fractions are taken from MC simulation and given in

Table 2: *B background modes considered in the $B^+ \to \rho^+\pi^0$ maximum likelihood fit. The second column gives the branching fractions used (estimated branching fractions are indicated by an asterisk), and the third column quotes the expected number of events entering into the sample, scaled to $81.5\,fb^{-1}$ (88.5×10^6 $\Upsilon(4S) \to B\overline{B}$ decays). The labels "long." and "tran." refer to the longitudinal and transverse polarization of the final states, respectively, in B decays into vector-vector mesons. $K_X^{(**)}$ refers to the higher kaonic resonances including $K_0^*(1430)$, $K_2^*(1430)$ and $K^*(1680)$. X_c indicates inclusive charmed decays.*

Mode	BR $[10^{-6}]$	N_{exp}
$B^0 \to \pi^0\pi^0$	1.6 ± 1.6	4.8 ± 4.8
$B^+ \to \pi^+\pi^0$	5.2 ± 0.8	5.6 ± 0.9
$B^+ \to K^+\pi^0$	12.7 ± 1.2	4.9 ± 0.5
$B^0 \to \rho^\pm\pi^\mp$	22.6 ± 2.8	44.6 ± 5.6
$B^0 \to \rho^- K^+$	7.3 ± 1.8	2.5 ± 0.6
$B^+ \to K_S^0(\pi^0\pi^0)\pi^+$	4.1 ± 0.4	5.4 ± 0.5
$B^0 \to K^{*0}(K^+\pi^-)\pi^0$	8.7 ± 5.0	3.8 ± 2.2
$B^0 \to K^{*0}(K_S^0\pi^0)\pi^0$	7.5 ± 5.0	3.9 ± 2.6
$B^+ \to K^{*+}(K^+\pi^0)\pi^0$	4.4 ± 2.5	6.1 ± 3.5
$B^+ \to \rho^+\gamma$	2.3 ± 2.3	1.3 ± 1.3
$B^0 \to \rho^+\rho^-$ long.	40.0^{+50*}_{-35}	64.8^{+81}_{-57}
$B^0 \to \rho^+\rho^-$ tran.	40.0^{+50*}_{-35}	$1.6^{+2.0}_{-1.4}$
$B^+ \to \rho^+\rho^0$ long.	$30.1^{+8.3}_{-9.9}$	$17.0^{+4.3}_{-5.2}$
$B^+ \to a_1^+\pi^0$	$35 \pm 35^*$	25.0 ± 25.0
$B^+ \to (K_X^{(**)}\pi)^+$	$40 \pm 26^*$	15 ± 9.8
$B^+ \to (K_X^{(**)}\rho)^+$	$20 \pm 20^*$	1.2 ± 1.2
$B^0 \to (K_X^{(**)}\pi)^0$	$72 \pm 54^*$	23 ± 17.3
$B^0 \to (K_X^{(**)}\rho)^0$	$20 \pm 20^*$	6.0 ± 6.0
Total charmless background		236.5 ± 79.3
$B^0 \to X_c^0$	–	72.0 ± 16.0
$B^+ \to X_c^+$	–	133.0 ± 30.0
Total B background		442 ± 86

Table 3: *B background modes considered in the $B^+ \to \rho^0\pi^+$ maximum likelihood fit. The second column gives the branching fractions used (estimated branching fractions are indicated by an asterisk), and the third column quotes the expected number of events entering into the sample, scaled to $81.5\,fb^{-1}$ (88.5×10^6 $\Upsilon(4S) \to B\overline{B}$ decays).*

Mode	BR $[10^{-6}]$	N_{exp}
$B^0 \to \rho^\pm\pi^\mp$	22.6 ± 2.8	29.3 ± 5.2
$B^0 \to \rho^- K^+$	7.3 ± 1.8	1.1 ± 0.3
$B^+ \to \rho^0 K^+$	3.9 ± 1.2	4.9 ± 1.5
$B^+ \to f_0(980)K^+$	11.7 ± 4.0	1.1 ± 0.4
$B^+ \to K^0_S(\pi^+\pi^-)\pi^+$	9.0 ± 0.9	5.3 ± 0.5
$B^0 \to K^{*+}(K^+\pi^0)\pi^-$	8.7 ± 5.0	1.4 ± 0.8
$B^+ \to K^{*0}(K^+\pi^-)\pi^+$	10.3 ± 2.6	11.1 ± 2.8
$B^+ \to \pi^+\omega(\pi^+\pi^-)$	0.14 ± 0.04	3.6 ± 1.0
$B^0 \to \rho^+\rho^-$ long.	40^{+50*}_{-35}	$6.3^{+7.8}_{-5.5}$
$B^0 \to \rho^0\rho^0$ long.	$3.5 \pm 3.5^*$	1.7 ± 1.7
$B^+ \to \rho^+\rho^0$ long.	$30.1^{+8.3}_{-9.9}$	$7.9^{+2.2}_{-2.6}$
$B^+ \to \eta'(\rho^0\gamma)\pi^+$	$3.0 \pm 2.0^*$	2.2 ± 1.5
$B^0 \to a_1^+\pi^-$	$35 \pm 35^*$	5.3 ± 5.3
$B^+ \to (K_X^{(**)}\pi)^+$	$40 \pm 26^*$	2.9 ± 1.9
$B^0 \to (K_X^{(**)}\pi)^0$	$72 \pm 54^*$	7.4 ± 5.5
Total charmless background	-	91.5±11.3
$B^0 \to X_c^0$	-	19.2 ± 5.8
$B^+ \to X_c^+$	-	54.1 ± 13.1
Total B background	-	165 ± 19

Table 1. The m_{ES}, ΔE, and NN output PDFs for signal and B background are taken from the simulation except for the means of the signal PDFs for m_{ES} and ΔE in $B^+ \to \rho^0\pi^+$, which are free to vary in the fit.

The parameterizations of PDFs are discussed in the following.

- $\boldsymbol{m_{ES}}$. The distribution of correctly reconstructed signal is parametrized using a Crystal Ball function [7].

  The continuum background is described by an ARGUS shape function [8] with floating shape parameter ξ.

- $\boldsymbol{\Delta E}$. We use a Crystal Ball [7] function (sum of two Gaussians) for correctly reconstructed signal in $\rho^+\pi^0$ ($\rho^0\pi^+$ and $\rho^0\pi^0$), and the sum of two Gaussians for misreconstructed signal events.

Table 4: *B background modes considered in the $B^0 \to \rho^0\pi^0$ maximum likelihood fit. The second column gives the branching fractions used (estimated branching fractions are indicated by an asterisk), and the third column quotes the expected number of events entering into the sample, scaled to $81.9\,fb^{-1}$ (88.9×10^6 $\Upsilon(4S) \to B\overline{B}$ decays).*

Mode	BR $[10^{-6}]$	N_{exp}
$B^+ \to \pi^+\pi^0$	5.2 ± 0.8	1.4 ± 0.2
$B^+ \to K^+\pi^0$	12.7 ± 1.2	0.9 ± 0.1
$B^0 \to \rho^\pm\pi^\mp$	22.6 ± 2.8	16.9 ± 1.4
$B^0 \to \rho^- K^+$	7.3 ± 1.8	0.7 ± 0.2
$B^+ \to \rho^+\pi^0$	$15.0\ ^{+15}_{-10}*$	$15.8\ ^{+15.8}_{-10.5}$
$B^0 \to K^0_S(\pi^+\pi^-)\pi^0$	3.5 ± 0.5	5.0 ± 0.7
$B^0 \to f_0(980)\pi^0$	0.0 ± 3.0*	$0.0\ ^{+3.1}_{-0.0}$
$B^0 \to \pi^+\pi^-\pi^0$ (non-res.)	0.0 ± 5.0*	$0.0\ ^{+4.1}_{-0.0}$
$B^0 \to K^{*0}(K^+\pi^-)\pi^0$	8.7 ± 5.0*	13.6 ± 7.8
$B^0 \to K^{*0}((K\pi)^0)\gamma$	40.2 ± 2.7	1.7 ± 0.1
$B^0 \to \rho^+\rho^-$ long.	$40.0\ ^{+50}_{-35}*$	$10.9\ ^{+13.6}_{-9.5}$
$B^+ \to \rho^+\rho^0$ long.	$30.1\ ^{+8.3}_{-9.9}*$	$15.8\ ^{+4.4}_{-5.2}$
$B^+ \to a_1^+((\rho\pi)^+)\pi^0$	35.0 ± 25.0*	5.2 ± 3.7
$B^0 \to \eta'(\rho^0\gamma)\pi^0$	0.0 ± 1.0*	$0.0\ ^{+2.0}_{-0.0}$
$B^+ \to (K_X^{(**)}\pi)^+$	40 ± 26*	2.3 ± 1.5
$B^0 \to (K_X^{(**)}\pi)^0$	72 ± 54*	3.2 ± 2.4
Total charmless background	-	93.4 ± 23.9
$B^0 \to X_c^0$	-	23.8 ± 7.1
$B^+ \to X_c^+$	-	35.2 ± 10.6
Total B background		152 ± 27

Continuum background is modeled by a linear function with a slope that is free to vary in the fit.

- **NN output**. PDFs for correctly reconstructed and for misreconstructed signal events are taken from MC simulation and parameterized using empirical shape-fitting techniques [9]. A small discrepancy between data and MC is observed for the NN output distributions of control samples using fully-reconstructed $B^0 \to D^-\rho^+$ decays. This is accounted for in the systematic error evaluation.

  For $B^+ \to \rho^+\pi^0$ and $B^+ \to \rho^0\pi^+$ ($B^0 \to \rho^0\pi^0$), the PDFs describing the NN output for continuum events are parametrized by a third-order (fifth-order) polynomial with its parameters determined in the fit.

- $\boldsymbol{\Delta t}$ is used in the $B \to \rho^0\pi^0$ fit to improve the discrimination against continuum background. The distributions for correctly reconstructed signal, misreconstructed signal and B background events are treated as decays of neutral or charged B's, convoluted with a Δt resolution function which is the sum of three Gaussians with parameters determined from a fit to fully reconstructed B decays [2]. This treatment does not introduce a bias in the signal yield according to MC studies.

  The continuum Δt distribution is parameterized as the sum of three Gaussian distributions with common mean, two relative fractions, and three distinct widths that scale the Δt event-by-event error, yielding six free parameters.

The shapes of the B background PDFs are obtained from MC simulation and parameterized using empirical shape-fitting techniques [9].

We perform fits on large MC samples with the measured proportions of signals and continuum and B backgrounds. Biases observed in these tests are due to imperfections in the likelihood model, *e.g.*, unaccounted correlations between the discriminating variables of the signal and B background PDFs. The observed signal yields are corrected for these fit biases and the full correction is assigned as a systematic uncertainty.

7 Preliminary Results

We obtain the event yields 170.8 ± 28.7(stat.) for $\rho^+\pi^0$, 232.5 ± 26.4(stat.) for $\rho^0\pi^+$ and 15.6 ± 11.7(stat.) for $\rho^0\pi^0$. Assuming equal branching fractions for $\Upsilon(4S)$ decays into neutral and charged B mesons, the yields translate into the branching fractions

$$\begin{aligned}
\mathcal{B}(B^+ \to \rho^+\pi^0) &= (11.0 \pm 1.9\ (\text{stat.}) \pm 1.9\ (\text{syst.})) \times 10^{-6}\ , \\
\mathcal{B}(B^+ \to \rho^0\pi^+) &= (9.3 \pm 1.0\ (\text{stat.}) \pm 0.8\ (\text{syst.})) \times 10^{-6}\ , \\
\mathcal{B}(B^0 \to \rho^0\pi^0) &< 2.5 \times 10^{-6} \text{ at } 90\% \text{ C.L.}\ ,
\end{aligned}$$

where the first errors are statistical and the second systematic. We find the charge asymmetries:

$$\begin{aligned}
A_{CP}^{\rho^+\pi^0} &= 0.23 \pm 0.16\ (\text{stat.}) \pm 0.06\ (\text{syst.}), \\
A_{CP}^{\rho^0\pi^+} &= -0.17 \pm 0.11\ (\text{stat.}) \pm 0.02\ (\text{syst.}).
\end{aligned}$$

Figure 1 shows distributions of m_{ES}, ΔE, the NN output and the ρ mass for $B^+ \to \rho^0\pi^+$, enhanced in signal content by cuts on the signal-to-continuum likelihood ratios of the other discriminating

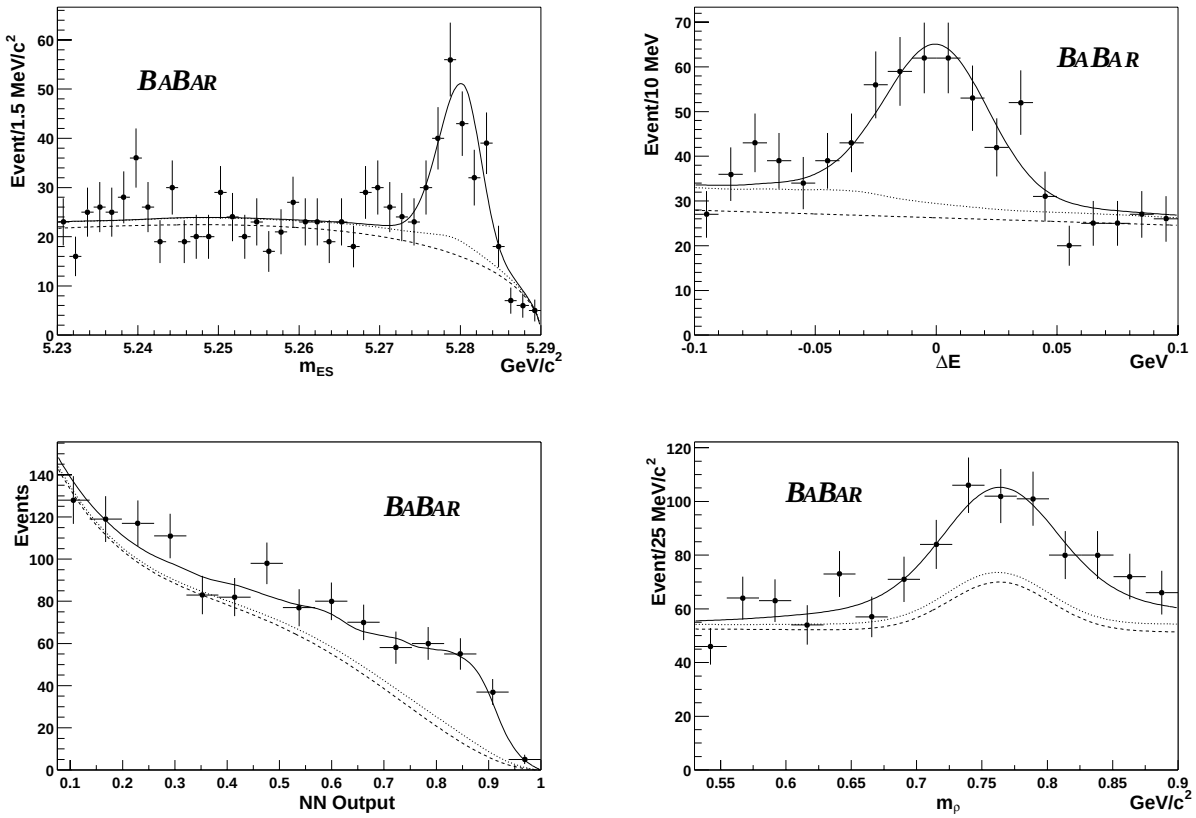

Figure 1: *Distributions of m_{ES} (upper left), ΔE (upper right), NN output (lower left) and the ρ mass (lower right) for samples enhanced in $\rho^0\pi^+$ signal content using cuts on the signal-to-continuum likelihood ratio. The solid curves represent projections of the fit result. The dashed curves represent the contribution from continuum events, and the dotted lines indicate the combined contributions from continuum events and B backgrounds. For the ρ mass distribution, the fit has been repeated with ρ-related information removed from the NN.*

variables. The plots of m_{ES}, ΔE and NN correspond to the fit reported here, while the plot of the ρ mass is obtained from a fit with ρ-related information removed from the NN.

The statistical significance of the previously unobserved $B^+ \to \rho^+\pi^0$ signal amounts to 9.4σ, which reduces to 6.6σ when also considering systematic errors. Figure 2 shows the corresponding signal-enhanced distributions of m_{ES} and ΔE.

For $B^0 \to \rho^0\pi^0$, a 90% confidence-level upper limit of 33.2 is obtained on the signal yield using a limit setting procedure similar to Ref. [10]. To obtain an upper limit for the branching ratio, the upper limit on the signal yield is shifted upwards by one sigma of the systematic error on the yield, and the efficiency and other scaling factors are shifted downwards by one sigma of their systematic errors. Figure 3 shows the corresponding signal-enhanced distributions of m_{ES} and ΔE.

All results are given in Tables 5 and 6 together with the systematic uncertainties discussed below.

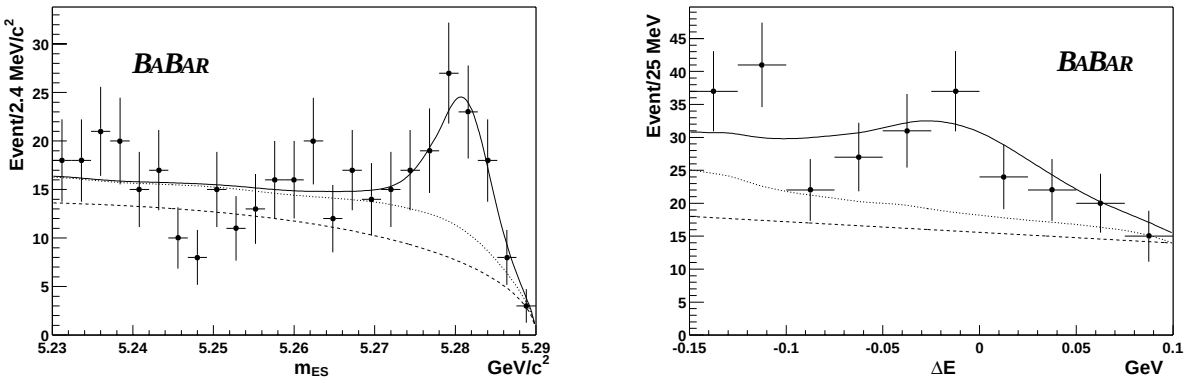

Figure 2: *Distributions of m_{ES} (left) and ΔE (right) for samples enhanced in $\rho^+\pi^0$ signal content using cuts on the signal-to-continuum likelihood ratio. The solid curves represent projections of the fit result. The dashed curves represent the contribution from continuum events, and the dotted lines indicate the combined contributions from continuum events and B backgrounds.*

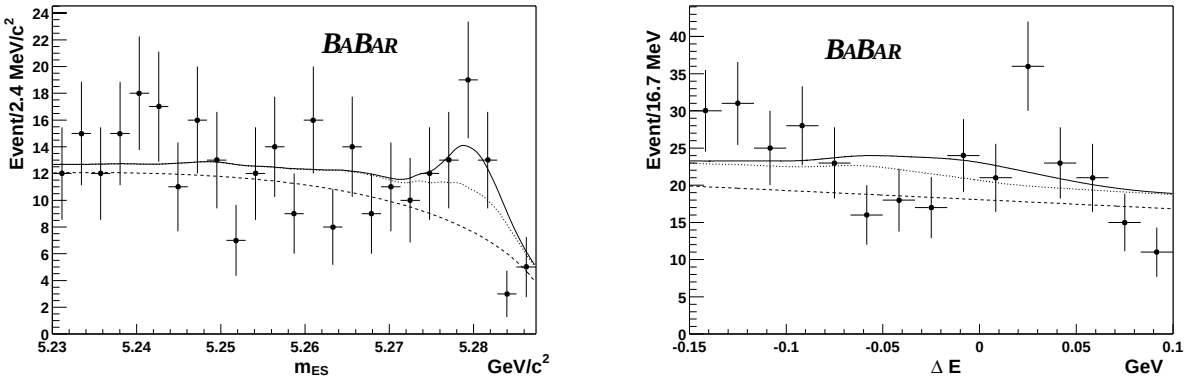

Figure 3: *Distributions of m_{ES} (left) and ΔE (right) for samples enhanced in $\rho^0\pi^0$ signal content using cuts on the signal-to-continuum likelihood ratio. The solid curves represent projections of the fit result. The dashed curves represent the contribution from continuum events, and the dotted lines indicate the combined contributions from continuum events and B backgrounds.*

8 Systematic Uncertainties

The systematic errors in the branching fractions are obtained by adding in quadrature the systematic uncertainties in the signal yields, the systematic uncertainties in efficiencies of tracking, particle identification, π^0 reconstruction and the systematic uncertainties on the selection cuts. The systematic errors on the A_{CP} measurements are introduced by the uncertainties in the treatment of the B background and by possible charge biases of the detector.

The basis for evaluating the systematic uncertainties on the cuts that are applied in the selection process is the differences in ΔE, m_{ES} and NN between on-resonance data and Monte Carlo simulation. The differences between data and Monte Carlo distributions of ΔE and m_{ES} are extracted from various fully-reconstructed B control samples for the three decay modes. The number of DIRC photons cut for the bachelor track in $B^+ \to \rho^0\pi^+$ decay mode will cause 1.0% uncertainty on the signal yield. The corrections and uncertainties on the signal efficiencies are summarized in Table 5 for the three decay modes.

We evaluate the systematic uncertainties due to the signal m_{ES}, ΔE and NN PDFs with a large B data control sample. The small differences observed in the distribution shapes for Monte Carlo events and the distribution shapes obtained from the data control sample are used to estimate the systematic uncertainty on the signal m_{ES} and ΔE PDFs. The uncertainties due to the estimated fractions of misreconstructed events are obtained from a control sample of fully-reconstructed $B \to D^-\rho^+$ decays as in Ref. [1]. We perform fits on the large MC samples with the measured proportions of $\rho^+\pi^0$, $\rho^0\pi^+$ and $\rho^0\pi^0$ signals, and continuum and B background. Fit biases observed in MC fits are added in quadrature and assigned as a systematic uncertainty of the fit procedure, referred to as "fitting procedure" in Table 5.

The expected yields from the background modes are varied according to the uncertainties in the measured or estimated branching fractions indicated in Tables 2, 3 and 4 for the $B^+ \to \rho^+\pi^0$, $B^+ \to \rho^0\pi^+$ and $B^0 \to \rho^0\pi^0$ decay modes, respectively. Since B background modes may exhibit direct *CP* violation, the corresponding parameters are varied within their physical ranges. Contributions from non-resonant $B^+ \to \pi^+\pi^0\pi^0$ for the $\rho^+\pi^0$ mode and $B^+ \to \pi^+\pi^-\pi^+$ for the $\rho^0\pi^+$ mode are negligible according to our dedicated studies. To check for these types of B backgrounds, a fit without ρ^0 mass and ρ^0 helicity information in its NN training is performed, and the results are compatible with the fit results reported here. The systematic error on the $\rho^0\pi^0$ yield due to non-resonant $B^0 \to \pi^+\pi^-\pi^0$ is considered as part of the B background one, based on Ref. [11].

For the $B^+ \to \rho^0\pi^+$ and $B^0 \to \rho^0\pi^0$ decay modes, systematic uncertainties due to possible interference between ρ^0 and $f_0(980)$ or a broad scalar $\sigma(400-1200)$ are estimated to be small. The orbital angular momentum for $\rho^0\pi^0$ ($\rho^0\pi^+$) is one, while for $f_0(980)\pi^0$ or $\sigma\pi^0$ ($f_0(980)\pi^+$ or $\sigma\pi^+$) it is zero. Therefore the two wave functions are orthogonal. The interference term vanishes when integrated over the whole space. As a cross check, MC samples with interference effects are made from non-resonant $B^+ \to \pi^+\pi^-\pi^+$ and $B^0 \to \pi^+\pi^-\pi^0$ Monte-Carlo using a reweighting technique. The full selection is then applied. The relative phase is chosen to maximize interference. Small effects are observed, as expected.

Table 5 summarizes the various sources contributing to the systematic errors in the branching fractions. The dominant systematic errors are due to the fit procedure (imperfection in likelihood model) and the uncertainties in the B background model. Table 6 summarizes the possible sources contributing to the systematic errors in the charge asymmetries.

Table 5: *Results and breakdown of systematic errors for the branching ratios measurements.*

	Signal yields and efficiencies		
	$B^+ \to \rho^+\pi^0$	$B^+ \to \rho^0\pi^+$	$B^0 \to \rho^0\pi^0$
Corrected signal yield	170.8	232.5	15.6
Corrected ϵ_{signal}	$17.5 \pm 0.1\%$	$28.3 \pm 0.1\%$	$20.0 \pm 0.1\%$
Statistical error on signal yield	28.7	26.4	11.7
	Yield systematics(absolute)		
$\tau_B \pm 0.016\,\text{ps}$	n/a	n/a	0.1
Δt resolution model	n/a	n/a	0.3
B tagging	3.7	n/a	0.9
Fraction of misreconstructed signal	3.0	1.3	0.1
ΔE PDF	8.5	0.7	1.0
m_{ES} PDF	2.5	1.6	1.5
NN PDF	3.0	3.2	2.6
B backgrounds	11.2	2.3	$^{+3.2}_{-3.9}$
Fitting procedure	14.4	8.2	6.3
Sub-total (absolute)	21.0	9.3	8.1
	Relative efficiency and scaling systematics		
Tracking efficiency correction	0.8%	2.4%	1.6%
PID for tracks	1.7%	5.2%	4.0%
Neutral correction	10.2%	n/a	5.1%
ΔE cut efficiency	2.6%	1.0%	0.1%
m_{ES} cut efficiency	0.0%	0.0%	0.0%
ρ cut efficiency	1.5%	0.0%	0.0%
NN cut efficiency	4.0%	4.0%	1.0%
DIRC photons cut for bachelor π^+	n/a	1.0%	n/a
$\mathcal{B}(\rho \to \pi^+\pi^-)$	1.6%	1.6%	1.6%
N($B\overline{B}$)	1.1%	1.1%	1.1%
Sub-total	11.6%	7.2%	7.0%
Total systematic error	16.9%	8.3%	52.5%
Branching ratio $[\times 10^{-6}]$	$11.0 \pm 1.9 \pm 1.9$	$9.3 \pm 1.0 \pm 0.8$	$0.9 \pm 0.7 \pm 0.5$

Table 6: *Results and breakdown of systematic errors for the measurements of charge asymmetries in* $B^+ \to \rho^+\pi^0$ *and* $B^+ \to \rho^0\pi^+$.

	$B^+ \to \rho^+\pi^0$	$B^+ \to \rho^0\pi^+$
A_{CP}	0.23	-0.17
Statistical error on A_{CP}	0.16	0.11
	Fit systematics	
B tagging	0.004	n/a
Fraction of misreconstructed signal	0.003	0.0012
ΔE PDF	0.034	0.0004
m_{ES} PDF	0.003	0.0016
NN PDF	0.00	0.0028
B backgrounds	0.050	0.022
Detector charge asymmetry	0.01	0.009
Total systematic error	0.06	0.02
$\boldsymbol{A_{CP}}$	$0.23 \pm 0.16 \pm 0.06$	$-0.17 \pm 0.11 \pm 0.02$

9 Summary

We have presented preliminary measurements of branching fractions and *CP*-violating charge asymmetries in $B^+ \to \rho^+\pi^0$ and $B^+ \to \rho^0\pi^+$ decays, and a search for the color-suppressed decay $B^0 \to \rho^0\pi^0$. The data sample used in the analyses consists of 89×10^6 $B\overline{B}$ pairs. We find a branching fraction for $B^+ \to \rho^0\pi^+$ that is consistent with previous measurements [12, 13]. We observe a signal for $B^+ \to \rho^+\pi^0$ with a significance of 6.6σ, and set an upper limit for $B^0 \to \rho^0\pi^0$. We do not observe evidence for direct *CP* violation.

10 Acknowledgments

We are grateful for the extraordinary contributions of our PEP-II colleagues in achieving the excellent luminosity and machine conditions that have made this work possible. The success of this project also relies critically on the expertise and dedication of the computing organizations that support *BABAR*. The collaborating institutions wish to thank SLAC for its support and the kind hospitality extended to them. This work is supported by the US Department of Energy and National Science Foundation, the Natural Sciences and Engineering Research Council (Canada), Institute of High Energy Physics (China), the Commissariat à l'Energie Atomique and Institut National de Physique Nucléaire et de Physique des Particules (France), the Bundesministerium für Bildung und Forschung and Deutsche Forschungsgemeinschaft (Germany), the Istituto Nazionale di Fisica Nucleare (Italy), the Foundation for Fundamental Research on Matter (The Netherlands), the Research Council of Norway, the Ministry of Science and Technology of the Russian Federation, and the Particle Physics and Astronomy Research Council (United Kingdom). Individuals have

received support from the A. P. Sloan Foundation, the Research Corporation, and the Alexander von Humboldt Foundation.

References

[1] *BABAR* Collaboration, B. Aubert *et al.*, hep-ex/0306030, submitted to Phys. Rev. Lett. (2003).

[2] *BABAR* Collaboration, B. Aubert *et al.*, Phys. Rev. **D66**, 032003 (2002);
BABAR Collaboration, B. Aubert *et al.*, Phys. Rev. Lett. **89**, 201802 (2002).

[3] Belle Collaboration, K. Abe *et al.*, Phys. Rev. **D66**, 071102(R) (2002).

[4] H.J. Lipkin, Y. Nir, H.R. Quinn and A. Snyder, Phys. Rev. **D44**, 1454 (1991).

[5] *BABAR* Collaboration, B. Aubert *et al.*, Nucl. Instrum. Methods **A479**, 1 (2002).

[6] Particle Data Group, K. Hagiwara *et al.*, Phys. Rev. **D66**, 010001 (2002).

[7] J.E. Gaiser *et al.*, Phys. Rev. **D34**, 711 (1986).

[8] ARGUS Collaboration, H. Albrecht *et al.*, Z. Phys. **C48**, 543 (1990).

[9] K.S. Cranmer, hep-ex/0011057, ALEPH 99-144 (1999)

[10] ALEPH, DELPHI, L3 and OPAL Collaborations, the LEP working group for Higgs boson searches, CERN-EP/98-046 (1998).

[11] *BABAR* Collaboration, B. Aubert *et al.*, hep-ex/0107058, LP01 Rome, *BABAR*-CONF-01/10 (2001).

[12] Belle Collaboration, A. Gordon *et al.*, Phys. Lett. **B542**, 183 (2002).

[13] CLEO Collaboration, C.P. Jessop *et al.*, Phys. Rev. Lett. **85**, 2881 (2000).